Visualizing metal-ion-binding sites in group I introns by iron(II)-mediated Fenton reactions

Christian Berens[1]*, Barbara Streicher[2], Renée Schroeder[2] and Wolfgang Hillen[1]

Background: Most catalytic RNAs depend on divalent metal ions for folding and catalysis. A thorough structure–function analysis of catalytic RNA therefore requires the identification of the metal-ion-binding sites. Here, we probed the binding sites using Fenton chemistry, which makes use of the ability of Fe^{2+} to functionally or structurally replace Mg^{2+} at ion-binding sites and to generate short-lived and highly reactive hydroxyl radicals that can cleave nucleic acid and protein backbones in spatial proximity of these ion-binding sites.

Results: Incubation of group I intron RNA with Fe^{2+}, sodium ascorbate and hydrogen peroxide yields distinctly cleaved regions that occur only in the correctly folded RNA in the presence of Mg^{2+} and can be competed by additional Mg^{2+}, suggesting that Fe^{2+} and Mg^{2+} interact with the same sites. Cleaved regions in the catalytic core are conserved for three different group I introns, and there is good correlation between metal-ion-binding sites determined using our method and those determined using other techniques. In a model of the T4 phage-derived *td* intron, cleaved regions separated in the secondary structure come together in three-dimensional space to form several metal-ion-binding pockets.

Conclusions: In contrast to structural probing with Fe^{2+}/EDTA, cleavage with Fe^{2+} detects metal-ion-binding sites located primarily in the inside of the RNA. Essentially all metal-ion-binding pockets detected are formed by tertiary structure elements. Using this method, we confirmed proposed metal-ion-binding sites and identified new ones in group I intron RNAs. This approach should allow the localization of metal-ion-binding sites in RNAs of interest.

Addresses: [1]Lehrstuhl für Mikrobiologie, Institut für Mikrobiologie, Biochemie und Genetik, Universität Erlangen-Nürnberg, Staudtstrasse 5, D-91058 Erlangen, Germany. [2]Institut für Mikrobiologie und Genetik, Universität Wien, Dr. Bohrgasse 9, A-1030 Vienna, Austria.

*Present address: Institut für Mikrobiologie und Genetik, Universität Wien, Dr. Bohrgasse 9, A-1030 Vienna, Austria.

Correspondence: Christian Berens
E-mail: berens@gem.univie.ac.at

Key words: Fenton chemistry, group I intron, metal-ion-binding site, ribozyme

Received: **4 November 1997**
Revisions requested: **11 December 1997**
Revisions received: **26 January 1998**
Accepted: **26 January 1998**

Published: **13 March 1998**

Chemistry & Biology March 1998, **5**:163–175
http://biomednet.com/elecref/1074552100500163

Introduction

Catalytic RNAs either require divalent cations for achieving a stable tertiary structure and for catalysis or their activity is greatly enhanced by the presence of divalent metal ions. Although abundant data exist on the influence of divalent metal ions on the structure and activity of RNA (for reviews, see [1–4]), only a few metal-ion-binding sites have been determined so far. They have primarily been identified crystallographically [5–9], or using phosphorothioate substitution [10–13], cleavage by various metal-hydroxyls [14–18] or photocleavage with uranyl acetate [19]. Unfortunately, these approaches have certain disadvantages. To date, the structures of only a few RNAs have been solved to high resolution using X-ray crystallography. Nuclear magnetic resonance (NMR) places size limits on the RNA to be analyzed and cannot detect Mg^{2+} ions. The photocleavage or chemical cleavage assays generate only a few cleaved sites. For example, Pb^{2+}-mediated cleavage of group I intron RNA leads to just two cleavage sites [16], although binding of at least three Mg^{2+} ions is required to generate a protected three-dimensional structure in an Fe^{2+}/EDTA footprint [20]. It would, therefore, be of advantage to have additional probes for metal-ion-binding sites.

Fe^{2+} can serve as such a probe. It is similar to Mg^{2+} both in size and coordination geometry [21], although the hard metal cation Mg^{2+} prefers oxygen ligands, whereas Fe^{2+}, as a softer metal cation, prefers nitrogen ligands [22]. Fe^{2+} would, thus, be expected to interact more strongly with the bases than Mg^{2+}. In the Fenton reaction, Fe^{2+} is oxidized in the presence of sodium ascorbate and hydrogen peroxide, thereby generating highly reactive hydroxyl radicals [23]. These diffusible agents can attack the ribose moiety, leading to cleavage of the nucleic acid backbone. The Fenton reaction has been widely employed in studying DNA conformation [24,25], protein–nucleic acid footprinting [26,27], DNA–drug interactions [28,29], and tertiary structure determination and folding of catalytic RNAs [20,30]. The Fenton reaction has also been used successfully to map metal-ion-binding sites in proteins like *Escherichia coli* glutamine synthetase [31], pigeon liver malic enzyme [32], and *E. coli* RNA polymerase [33], as well as in protein–ligand

complexes, such as pig heart NADP-specific isocitrate dehydrogenase with isocitrate [34], Tn*10* Tet repressor and tetracycline [35], *E. coli* RNA polymerase with T7A1 promoter DNA [36], and the homing endonucleases I-*Dmo*I and I-*Por*I with their DNA substrates [37]. Free Fe^{2+} has only rarely been used in RNA studies. Grosshans and Cech [38] showed that Fe^{2+} is not catalytically active in group I intron splicing. Wang and Cech [39] observed specific Fe^{2+}-mediated cleavage sites when the concentration of Fe^{2+} exceeded that of the metal ion chelator, whereas Zhong and Kallenbach [40] used it as a cationic probe for surface accessibility in tRNA and 5S rRNA tertiary structure.

In this paper, we describe Fe^{2+}-mediated RNA backbone cleavage to identify nucleotide positions close to metal-ion-binding sites in group I introns, the structurally and functionally best-characterized family of large catalytic RNAs. Group I introns contain a distinct inside and outside [30], the existing data on metal ions are profound [4,11,16,41–45], detailed three-dimensional models have been reported for three of the four subgroups of group I introns [18,46,47] and, recently, the crystal structure of the P4–P6 domain of the *Tetrahymena thermophila* LSU intron was solved [8,13,48]. We show that in the presence of Fe^{2+}, sodium ascorbate and hydrogen peroxide, five distinct regions that are conserved in the *td*, *sunY*, and *Tetrahymena* introns, are cleaved in the intron core. Additional cleavage sites are also observed in the respective peripheral elements. The majority of the Fe^{2+}-mediated cleavage signals detected are in the interior of the folded RNA. Cleaved regions, which are dispersed over the secondary structure of the T4 phage-derived *td* intron, come together in space to form several clear metal-ion-binding pockets in a three-dimensional model of the intron. The cleaved nucleotides are close to published metal-ion-binding sites [8,11,13,16,18].

Results and discussion

Monitoring the correct fold of the RNA

The native fold of the bacteriophage T4-derived *td*L-7 intron was monitored by Fe^{2+}/EDTA structure probing [30,49]. A representative result is shown in Figure 1. With *td*L-7 RNA denatured in the absence of Mg^{2+}, cleavage by Fe^{2+}/EDTA occurs fairly uniformly throughout the entire molecule (Figure 1a, lane 9), with a less than twofold difference in cleavage intensity. In contrast, with intron RNA renatured in the presence of 3 mM Mg^{2+}, cleavage in distinct regions is suppressed threefold to fourfold, to a maximum of sixfold (Figure 1a, lane 10). Comparison of these regions with the protected regions published by Heuer *et al.* [49] reveals a similar extent of protection from cleavage, and nearly identical protected regions (Figure 1b). These vary only by one or two nucleotides in length or position, despite the fact that the protection maps were obtained under highly different renaturation and reaction conditions. The renaturation conditions we employed (3 mM Mg^{2+} and 400 μM spermidine) are sufficient to ensure that the ribozyme obtains a correctly folded tertiary structure [50]. This is supported by the observation that, under our renaturation conditions, the *td*L-7 intron undergoes intramolecular cyclization (data not shown; see also [51]), a reaction requiring a correctly folded ribozyme [52]. We found two additional protected regions in the P7 extension (Figure 1b). They map to nucleotides C879–G883 in L7.1 and nucleotides A897–G898 in L7.2. The nucleotides in L7.2 are adjacent to the nucleotides forming the P12 tertiary contact [53]. The nucleotides in P9.2 that participate in this tertiary contact had already been observed to be protected from cleavage by Fe^{2+}/EDTA [49]. Taken together, these results demonstrate that the renatured ribozyme is folded correctly.

Fe^{2+} specifically cleaves native *td* intron RNA

In the absence of EDTA or other chelators, Fe^{2+} can replace Mg^{2+} in Mg^{2+}-binding sites in proteins and protein–ligand complexes [31–37]. Reasoning that this might also be the case for group I introns, we end-labelled *td*L-7 RNA and incubated renatured RNA with 250 μM Fe^{2+} and denatured RNA with 10 μM Fe^{2+} to identify Fe^{2+}-mediated cleavage sites. These concentrations of Fe^{2+} yielded about 70% full-length ribozyme (data not shown), which should ensure only a single cut per molecule [54]. The results are shown in Figure 1a and 1c. The controls without Fe^{2+} (Figure 1a, lanes 3, 4) show that cleavage is dependent on the presence of Fe^{2+}. For the cleavage reaction with Fe^{2+}, ten regions of differing cleavage intensity are easily detected in the native RNA (Figure 1a, lane 8). Strong cleavage sites map to J5/4, J6/7 and J8/7. Cleavage of intermediate strength is observed in J7.2/3 and L9, whereas weaker sites are located in J4/5, L6a, P7.1, P9.1 and L9.2. Cleaved regions span between one (L9, L9.2) and ten (L6a, J6/7) nucleotides, with a mean of about five nucleotides. The denatured RNA (Figure 1a, lane 7) has no reproducible cleavage sites (data not shown). The nucleotides cleaved were identified by comparison with an RNase T1 sequencing reaction and an alkaline hydrolysis ladder (see below). Hydroxyl radical cleavage of a nucleotide results in cleavage at the ribose, leading to elimination of the nucleoside [28]. A signal in the Fe^{2+} cleavage lane therefore corresponds to cleavage of the nucleotide at its 3′ side. We observed no bias for cleavage at any base; all four bases were cleaved to an equal extent. With respect to the secondary structure elements, nucleotides in loops are cleaved to the same extent as they are present in the ribozyme (18%). Nucleotides in paired regions are cleaved less frequently (42%) than they are present in the RNA (59%) and nucleotides in junctions are cleaved to a higher degree (40%) than their presence in the intron (23%).

Figure 1

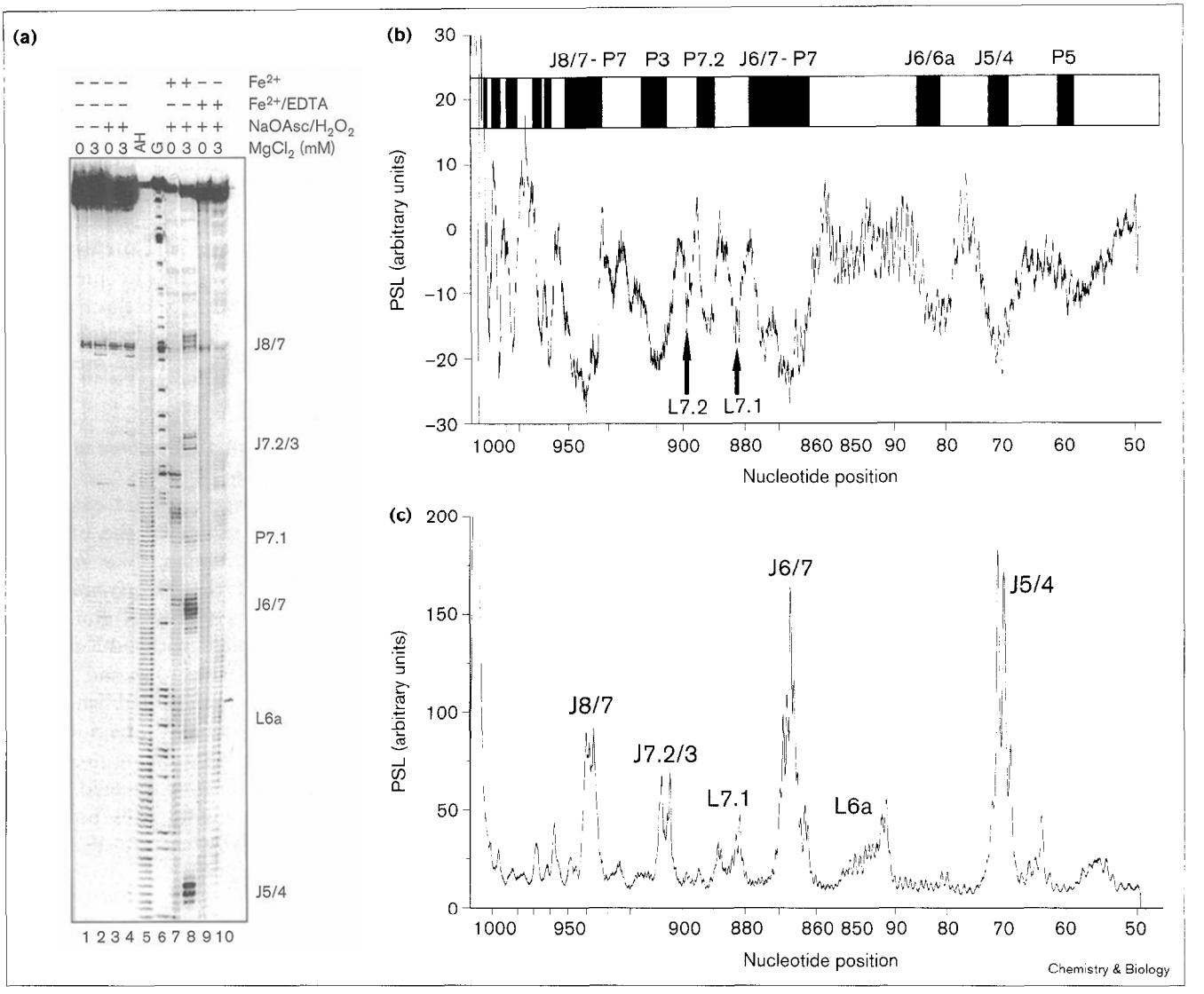

Mapping of the Fe^{2+} cleavage sites in the *td* RNA. **(a)** Autoradiogram of a 6% denaturing polyacrylamide gel with 5′ end-labelled *td*L-7 RNA cleaved by either 10 μM (lane 7) or 250 μM Fe^{2+} (lane 8), or by 250 μM Fe^{2+}/500 μM EDTA (lanes 9, 10). Controls with untreated RNA (lanes 1, 2) and in which Fe^{2+} was omitted (lanes 3, 4) are also shown. The respective final concentrations of Mg^{2+} in the reaction tubes, as well as the presence (+) or absence (–) of Fe^{2+}, sodium ascorbate (tenfold molar excess over Fe^{2+}), and hydrogen peroxide (tenfold molar excess over Fe^{2+}) are shown above each lane. The *td* secondary structure elements cleaved by Fe^{2+} are marked on the right. Sequencing markers are: AH (alkaline hydrolysis) and G (T1 ladder). Lanes 1, 3, 7 and 9 contain denatured, lanes 2, 4, 8 and 10 renatured intron RNA. Quantitation of **(b)** the Fe^{2+}/EDTA cleavage reactions and **(c)** the Fe^{2+} cleavage reactions. The polyacrylamide gel shown in (a) was quantitated in a phosphorimager. Nucleotide positions in the *td* RNA are given on the x axis and secondary structure elements that are either (b) protected from cleavage by Fe^{2+}/EDTA or that are (c) cleaved by Fe^{2+} are highlighted. The Fe^{2+}/EDTA panel in (b) shows the difference between cleavage in the presence of 3 mM Mg^{2+} and cleavage in the absence of Mg^{2+}. Valleys or troughs denote regions of protection, whereas peaks correspond to regions of cleavage. For comparison, the protected regions determined by Heuer *et al.* [49] are included as filled boxes in the panel. Additional protected regions that were not identified by Heuer *et al.* [49] are shown by filled arrows and the secondary structure elements in which they are located. PSL, photo-stimulated luminescence.

Mg^{2+} competes with Fe^{2+} for cleavage sites

Site-specific cleavage of RNA by divalent metal ions, such as Pb^{2+}, Ca^{2+}, and Sr^{2+}, is strongly influenced by the concentration of Mg^{2+}. High concentrations of Mg^{2+} displace these ions from the cleavage sites, indicating competition for the same or overlapping binding sites [5,16–18,55–57]. To determine if the Fe^{2+}-mediated cleavage sites are also competed for by Mg^{2+}, cleavage of native *td*L-7 RNA was performed with increasing amounts of $MgCl_2$. The Mg^{2+} concentrations employed should have no or only a slight effect on the efficiency of the Fenton reaction [58,59]. The results obtained are

Figure 2

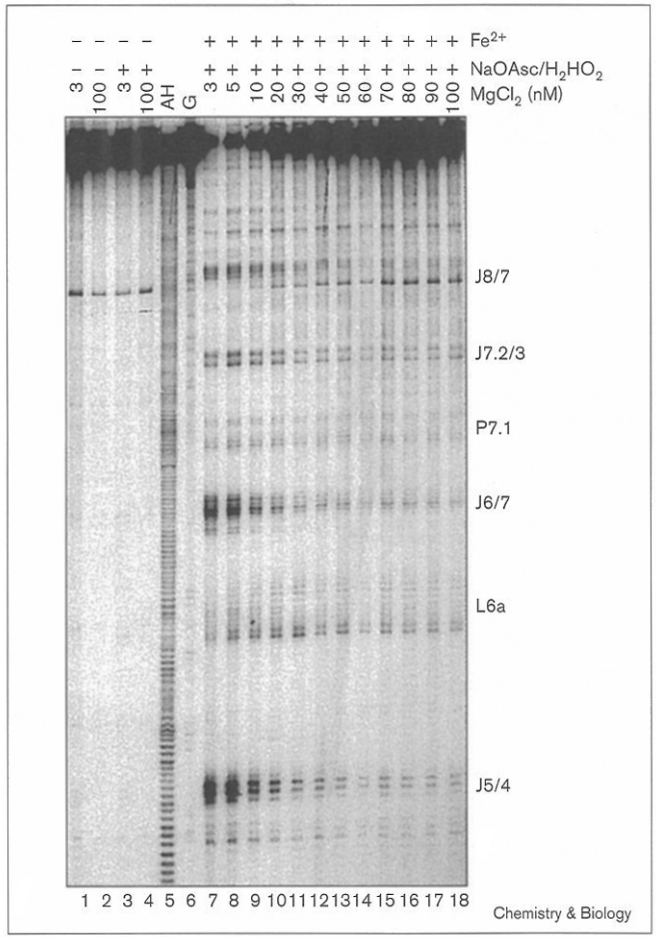

Mg^{2+}-competition of Fe^{2+}-cleavage in native *td* RNA. Autoradiogram of a 6% denaturing polyacrylamide gel with 5′ end-labelled renatured *td*L-7 RNA treated with 250 μM Fe^{2+} and increasing amounts of Mg^{2+}. Controls with untreated RNA (lanes 1, 2) and in which Fe^{2+} was omitted (lanes 3, 4) were also included. The respective final concentrations of Mg^{2+} in the reaction tubes (lanes 7–18), as well as the presence (+) or absence (–) of Fe^{2+}, 2.5 mM sodium ascorbate and 2.5 mM hydrogen peroxide are displayed above each lane. The *td* secondary structure elements cleaved by Fe^{2+} are marked on the right. Sequencing markers are AH (alkaline hydrolysis) and G (T1 ladder).

shown in Figure 2. The extent of cleavage by Fe^{2+} is reduced for all cleavage sites and reaches a minimum plateau at 30–40 mM $MgCl_2$, indicating that both metal ions compete for identical or overlapping binding sites. This corresponds to the data obtained for Pb^{2+}-mediated cleavage of *td* [16] and RNase P RNA [17], in which only residual cleavage by Pb^{2+} was observed in the presence of more than 30 mM $MgCl_2$. Quantitation using phosphorimager analysis shows that the reduction of cleavage is most pronounced for the strongest sites in the regions J5/4 and J6/7 with an approximately tenfold reduction in signal strength. The competition is weaker at the cleavage sites in J7.2/3 and J8/7 and least for those in L6a and P7.1 with sixfold and threefold reductions, respectively.

Zhong and Kallenbach [40] used Fe^{2+} as a cationic surface probe for RNA tertiary structure. Using their reaction conditions, the ratio of Fe^{2+} to Mg^{2+} was 1:70 which would correspond roughly to the lane with 20 mM Mg^{2+} in Figure 2. There, the Fe^{2+} cleavage signals are already quite weak, but can still be detected. Zhong and Kallenbach [40] did observe positions with strong cleavage by Fe^{2+} in tRNA (one position) and 5S rRNA (three positions). They are adjacent to or within regions protected from cleavage by Fe^{2+}/EDTA and/or Fe^{2+}/EDDA. In the tRNA, the strong Fe^{2+} cleavage site is also cleaved by Pb^{2+} and is close to a metal-ion-binding site present in several crystal structures [5,55]. Two of the three sites in the 5S rRNA are cleaved by Pb^{2+} [60] and might, thus, correspond to positions close to one or more metal-ion-binding site(s).

Fe^{2+} cleaves the same sites in the ribozyme cores of the *sunY* and *Tetrahymena* LSU introns

To investigate if the Fe^{2+} cleavage sites are conserved among group I introns, we also examined the bacteriophage T4-derived *sunY* intron, which, like *td*, is a member of the IA2 group, and the *Tetrahymena thermophila* LSU intron which belongs to the IC1 group [61]. Figure 3 shows the results obtained with both introns. Their Fe^{2+}/EDTA footprints (lanes 11 and 12 in Figure 3a and 3b) are very similar to those published previously [20,30,49,62]. The additional protection sites observed in L7.1 and L7.2 of the *td* intron are present in the *sunY* intron and are slightly more pronounced. In the *Tetrahymena* ribozyme, we observed no sites protected from Fe^{2+}/EDTA cleavage other than those already published [49].

For *sunY*, the Fe^{2+}-cleavage sites are also conserved. This becomes clear by comparing the exact nucleotides cleaved in *td* (shown in Figure 4) with those cleaved in *sunY* (Figure 5). Except for J4/5 and L5, all regions cleaved in the *td*L-7 RNA are cleaved in *sunY*L-13, although the extent and intensity of cleavage vary (compare L6a and J5/4 in Figures 1a and 3a). In general, the extent of Fe^{2+}-mediated cleavage is similar to that observed for *td*. Cleavage sites span from one (L9, P9.1a, L9.2) to 12 nucleotides (L7.1), with a mean of four. Several additional cleavage sites are present in the P9 extension.

The Fe^{2+} cleavage sites determined for the *Tetrahymena* ribozyme are shown in Figure 6. They span from one (many occasions) to nine (J6/7) with a mean of only two. The cleavage sites in the intron core are conserved. The cleavage site in L6a is not present in the *Tetrahymena* ribozyme. Most of the other cleavage sites are in the P5abc extension. There are five nucleotides cleaved in the A-rich bulge surrounding the two Mg^{2+}-binding sites determined in the crystal structure of the *Tetrahymena* P4–P6 domain [8]. Phosphate oxygens from the cleaved

Figure 3

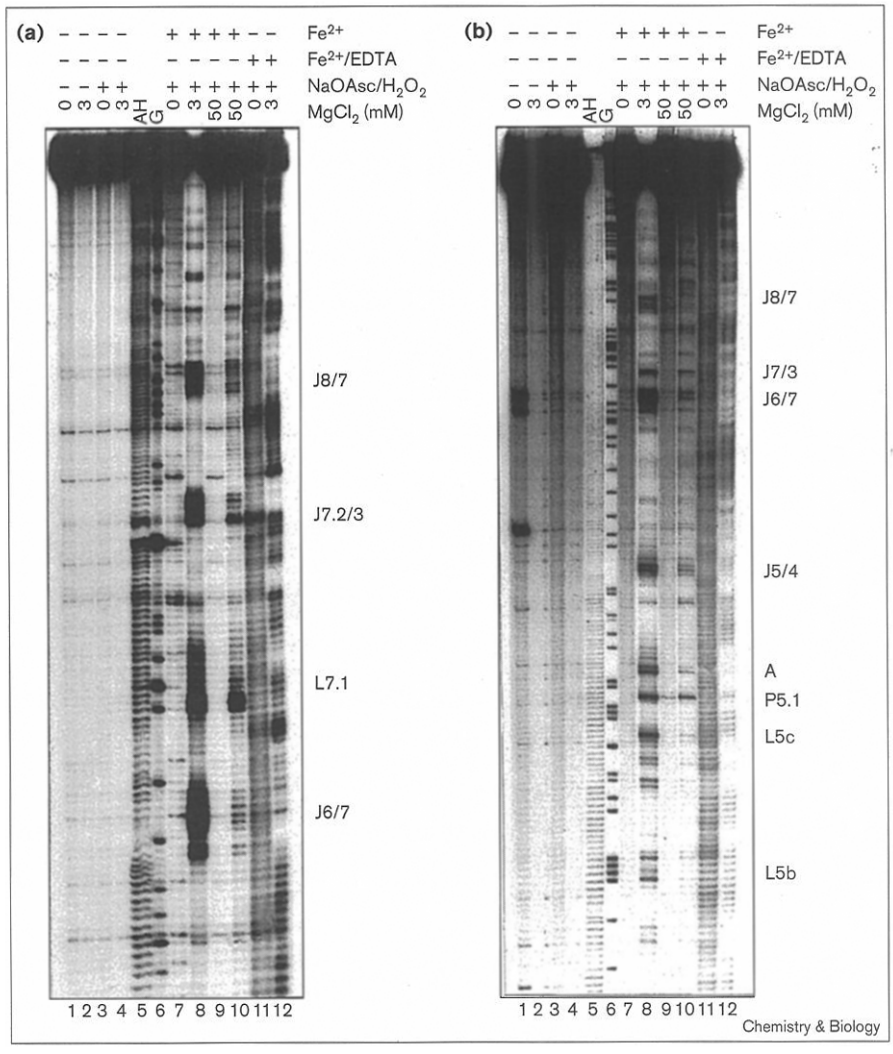

Mapping of the Fe^{2+} cleavage sites in the *sunY* and in the *Tetrahymena thermophila* LSU RNAs. Autoradiograms of 6% denaturing polyacrylamide gels with 5′ end-labelled **(a)** *sunY*L–13 RNA and **(b)** *Tetrahymena* L–21 RNA cleaved by 10 μM Fe^{2+} (lanes 7, 9), 250 μM Fe^{2+} (lane 8, 10) or by 250 μM Fe^{2+}/500 μM EDTA (lanes 11, 12). Controls with untreated RNA (lanes 1, 2) and in which Fe^{2+} was omitted (lanes 3, 4), as well as competition of Fe^{2+} cleavage by 50 mM Mg^{2+} (lanes 9, 10) are also shown. The respective final concentrations of Mg^{2+} in the reaction tubes (lanes 7–12), as well as the presence (+) or absence (–) of Fe^{2+}, sodium ascorbate (tenfold molar excess over Fe^{2+}), and hydrogen peroxide (tenfold molar excess over Fe^{2+}) are displayed above each lane. Renatured RNA is in lanes 2, 4, 8, 10 and 12, denatured RNA in lanes 1, 3, 7, 9 and 11. The *sunY* and *Tetrahymena* secondary structure elements cleaved by Fe^{2+} are marked on the right and the A-rich bulge in *Tetrahymena* as presented in Cate *et al.* [8] is indicated by a bold capital A. Sequencing markers are AH (alkaline hydrolysis) and G (T1 ladder).

nucleotides A184 and A187 are directly coordinated to the Mg^{2+} ions [13].

Fe^{2+}-cleavage sites are located primarily in the RNA interior

Figure 7 shows a comparison of the cleavage sites obtained using Fe^{2+} and those obtained using Fe^{2+}/EDTA. Most of the sites cleaved, except for those in L6a, are embedded in regions protected from cleavage by Fe^{2+}/EDTA or border them (see also Figure 1). They are located in the interior of the RNA where one would expect them to be if the metal ions they reflect bury phosphate oxygens in the RNA interior [13]. Figure 7 also shows the theoretical accessibility of the C4′ positions to Fe^{2+}/EDTA in the three-dimensional model of the entire *td* intron [18]. It correlates very well with the experimentally determined accessibility to Fe^{2+}/EDTA. The sole exception is in L7.1 in which we observe an additional protected region in the *td* RNA. The three-dimensional model is therefore a good starting point to search for metal-ion-binding sites in *td*.

The Fe^{2+}-cleavage sites come together in space to form pockets

Figure 8a shows a stereoview of the three-dimensional model of the entire *td* intron with the proposed binding sites for the metal ions A (yellow) and B (orange) in the catalytic core [18]. In this model, most of the cleavage sites determined for Fe^{2+} come together in three-dimensional space to form several pockets where metal ions might be bound. These putative metal-ion-binding pockets are color-coded in Figure 4 and include cleavage sites corresponding to the metal-ion-binding sites A (yellow) and B (orange) [18], P5 and L9 (blue), close to the L9/P5 tertiary contact [63], P6a and L6a (light green), P6 and J8/7 (purple), L7.1 and J7.2/3 (pink), P7.1 and J7.1/7.2 (dark blue), and also between J7.2/3 and J8/7 (grey). The most striking observation is that, except for the cleavage sites in P6a and L6a and those in P7.1 and J7.1/7.2, and in J8/7, these pockets are formed by nucleotides that are widely separated in primary and

Figure 4

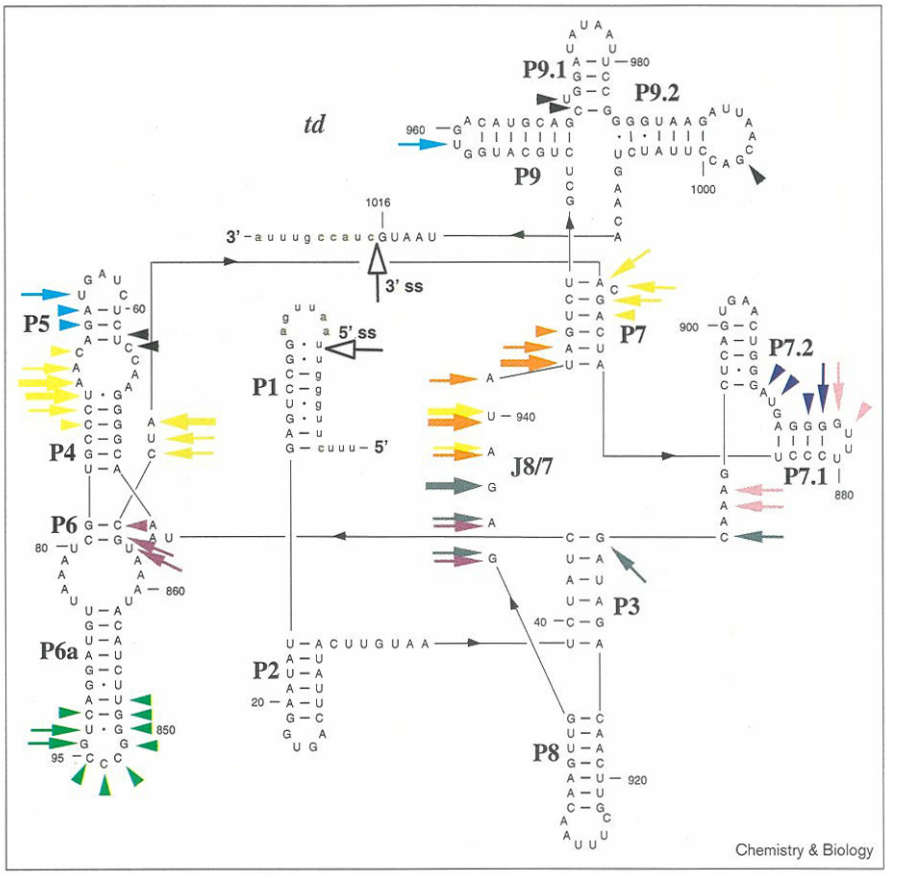

Fe^{2+} cleavage sites in group I intron RNAs. Secondary structure of the T4 phage-derived *td* intron (from Streicher *et al.* [18]). The paired regions [76] are marked and the splice sites are indicated by open arrows. Nucleotides belonging either to exon sequences or that were deleted from the 5′ end of the intron are in lower case. Nucleotides in which Fe^{2+}-mediated cleavage of the RNA backbone is observed are shown with a filled arrowhead when only weak cleavage is detected at the site, by filled arrows at sites with intermediate cleavage intensity, and by bold, filled arrows at sites of strong cleavage. The color coding of the Fe^{2+}-mediated cleavage sites represents putative metal-ion-binding pockets in the three-dimensional model of the intron [18]. Cleavage sites that are close to each other in space and could, thus, form a metal-ion-binding pocket are shown in identical colors, whereas cleavage sites that could not be assigned to distinct binding pockets are shown in black. For cleavage sites in J8/7 that can be assigned simultaneously to two different binding pockets (orange/yellow or purple/grey), arrows are displayed for both pockets in their respective colors.

secondary structure and, therefore, represent tertiary interactions. This is consistent with crystal structures [5,7,8,55] in which metal ions bridge separate RNA strands and the observation that, in the absence of Mg^{2+}, the secondary structure of group I introns is mostly formed, while no, or only little, tertiary structure is present [20,64]. Figure 8b shows the catalytic core of the intron with the metal ions A and B as viewed from the substrate helix P1. The C4′-atoms of the nucleotides cleaved by Fe^{2+} are highlighted by cyan spheres. All strong cleavage sites, except G938, as well as the medium cleavage sites in J6/7, in J8/7, and in J7 are within 10 Å of one of these ion positions. They nicely form pockets around each of the two metals. Two pockets for metal ions are formed by residues from J8/7. McConnell *et al.* [44] proposed recently that one or more high affinity metal-ion-binding sites, which they named 'site 4', might be located in J8/7. These metal ions are involved in retaining the P1 substrate helix in the catalytic core of the ribozyme. Residues in the 3′-half of J8/7 come close to P1 [61]; A302 in the *Tetrahymena* ribozyme interacts, for example, with the 2′-hydroxyl of –3U in a substrate helix replacing P1 [65]. Mutation of residues A301–G303 to CGC in the *Tetrahymena* ribozyme results in a molecule that has all the properties expected for a mutant impaired in the correct binding of the P1 helix [66]. In the presence of a substrate oligonucleotide, residues in J8/7 of the *Tetrahymena* ribozyme are protected from cleavage by Ca^{2+} [44] and from modification by DMS [65]. It is, therefore, tempting to speculate that the pockets formed with residues in J8/7 might represent these site 4 ion-binding site(s).

The Fe^{2+} cleavage data correlate with phosphorothioate substitution, metal-hydroxyl cleavage and X-ray crystallography data

Phosphorothioate substitution

Phosphorothioate substitution of the pro-Rp oxygen in the *Tetrahymena* intron identified 37 positions leading to reductions in either 3′ splice site hydrolysis [41] or the rate of addition of the cofactor guanosine to the 5′-end of the intron [11]. 'Manganese rescue' identified 11 phosphates (5′ to positions G201, A206, A207, U258, U259, A261, G264, A268, U305, A306 and A308) as coordination sites for divalent metal ions [11]. Seven sites in phosphorothioate-substituted *Tetrahymena* P4–P6 domain RNA disrupted folding as assayed by electrophoresis in native gels [13]. Six of these (5′ to positions G163, A171, A184, A186, A187 and G188) coordinate Mg^{2+} ions in the P4–P6 crystal structure [8]. With the exception of A186, G201 and A268, nucleotides bordering all of these coordinating phosphates

Figure 5

Secondary structure of the T4 phage-derived *sunY* intron (from Cech *et al.* [77]; modified because of the deletion of nucleotides U210–C990). The legend is as for Figure 4, except that the cleavage sites are not color coded.

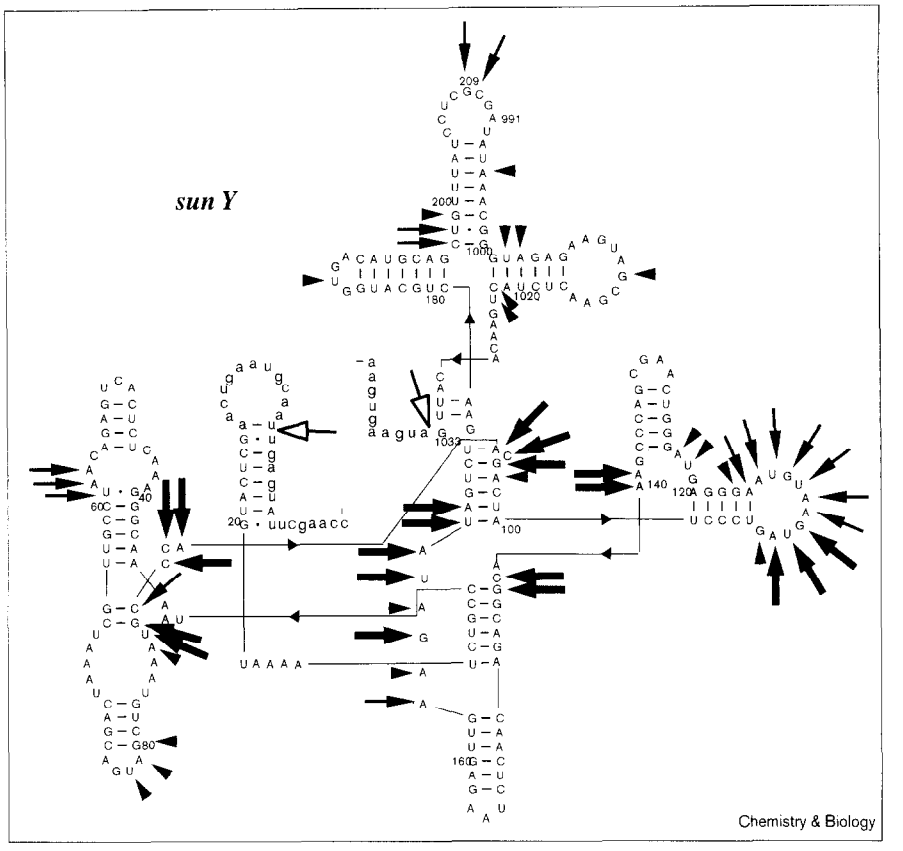

are also cleaved by Fe^{2+} (Figure 6). Cleavage sites for Fe^{2+} were also found for many of the other phosphorothioate interference sites, as can be seen in Figure 6. The correlation is good for cleavage sites in the P4–P6 domain and in the catalytic core. There are several phosphorothioate interference sites in the P2 extension and two in J9.1a/9.1 in which we find no Fe^{2+}-mediated cleavage sites.

Metal-hydroxyl cleavage

Cleavage of the *td*, *sunY* and *Tetrahymena* introns with Pb^{2+} yielded conserved sites 5′ to the bulged nucleotide in P7 and U305 in J8/7 (numbering according to the *Tetrahymena* intron), with additional minor sites in the *sunY* intron (5′ to A306 in J8/7 and A308 in P7). Incubation of the *td* intron with Ca^{2+}, Sr^{2+} and Mn^{2+} resulted in core cleavage 5′ to U940 in J8/7 (which corresponds to U305 in *Tetrahymena*) [16,18]. These nucleotides are all cleaved by Fe^{2+}.

X-ray crystallography

Recently, the crystal structure of the P4–P6 domain of the *Tetrahymena thermophila* LSU intron was solved [8,13,48]. Each of the two molecules in the asymmetric unit contains 12 Mg^{2+} ions and two cobalt hexammine ions in P5b and P5c. Five of the Mg^{2+} ions, located in the three-helix junction and the A-rich bulge, can be replaced by Mn^{2+}. The Mg^{2+} and cobalt hexammine ions detected are shown in Figure 9a, together with the C4′ positions of nucleotides cleaved by Fe^{2+}. The abundance of Mg^{2+} ions found makes it clear that the assignment of Fe^{2+} cleavage signals to metal-ion-binding pockets is not straightforward. In Figure 6, all Fe^{2+}-cleavage sites in the P4–P6 domain that are within 10 Å of a metal ion are colored blue which covers most of the cleavage sites obtained with Fe^{2+}. Figure 9b shows the A-rich bulge. Fe^{2+}-generated cleavage sites flank the two metal ions. The majority of cleavage sites that are not in the proximity of a metal-ion-binding site are at the interface with the rest of the intron. Cleavage sites within J5/5a that are not close to a Mg^{2+} ion, but are close to a phosphorothioate interference site form a pocket in the RNA crystal structure. Another site of interest is the tetraloop and its receptor. Several residues participating in this tertiary contact are cleaved by Fe^{2+} and inspection of Figure 4 in Cate *et al.* [8] shows a pocket that might accomodate a metal ion. We would like to point out that the L9/P5 tertiary interaction in *td* also involves a GNRA tetraloop (see Figure 4). The metal-ion-binding sites in P5, bridging P5 and P5a, and between P5b and P6a did not yield any Fe^{2+}-mediated cleavage sites. The ions at these sites were not replaced by Mn^{2+} [13] which, according to the authors, could have been due to the spermidine present in the crystallization medium. As our cleavage assay buffer also contains

Figure 6

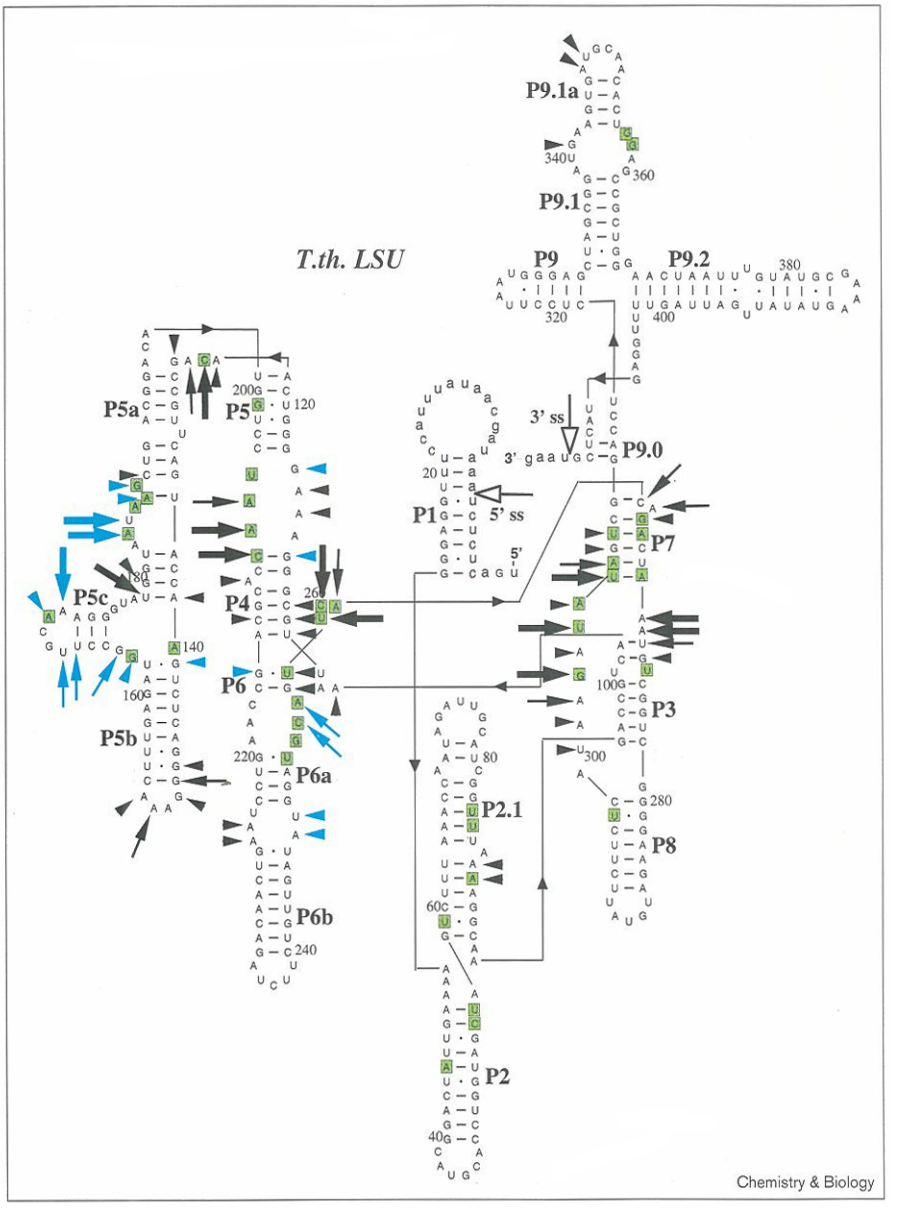

Secondary structure of the *Tetrahymena thermophila* LSU intron (from Cech *et al.* [77] and Cate *et al.* [8]). The legend is as for Figure 4, except that the cleavage sites are not color coded. Cleaved nucleotides in the P4–P6 domain (nucleotides A104–A261) with ribose C4′ atoms < 10 Å away from a metal ion position in the crystal structure are indicated by blue arrows. Nucleotides in which the presence of a pro-Rp phosphorothioate leads to reduction in catalytic activity [11,41] or to loss of folding [13] are highlighted by filled green squares.

spermidine, this might be a reason for the lack of cleavage sites at these metal-ion positions. Two metal-ion-binding sites were identified in the major groove of the RNA [48,67] and mapped to P5b and P5c. The metal ion bound in P5b contacts the guanines at positions 147 and 148 and comes close to the phosphate groups; we observe slightly shifted cleavage sites at positions 148–150. In the P5c helix, a hydrated metal ion contacts phosphate oxygen atoms at positions 174 and 175. There are no Fe^{2+}-mediated cleavages at these positions. This makes it clear that the identification of metal-ion-binding sites in the major groove will be difficult if only RNA backbone cleavage is assayed. Additional information on these binding pockets will have to come from Fe^{2+}-dependent cleavage at the bases. Fe^{2+} can attack the bases of 2′-deoxynucleotides or single-stranded DNA leading to, among other damage products, base loss and ring opening, as has been shown for single-stranded DNA [68] and, in more detail, the deoxyguanosine and deoxycytosine families [69,70]. In analogy, Fenton cleavage of RNA at the bases should also yield products that can be detected by aniline cleavage or primer extension.

Overall, the correlation between the published data on metal-ion-binding sites in group I introns and our Fe^{2+} cleavage data is very good, demonstrating that the method presented in this paper is capable of identifying a subset of metal-ion-binding sites in RNA. It should be generally

Figure 7

Theoretical and experimental solvent accessibility of C4′ positions in the *td* intron model. The theoretical solvent accessibilities of the C4′ positions to Fe^{2+}/EDTA were calculated by Eric Westhof and co-workers [18] for the entire *td* intron model with ACCESS [78] using a sphere radius of 2.8 Å. Nucleotides cleaved by Fe^{2+}/EDTA experimentally are indicated by open circles and nucleotides protected from cleavage by Fe^{2+}/EDTA by filled circles. Nucleotides cleaved by Fe^{2+} are shown as red circles, whereas nucleotides that are protected from cleavage by Fe^{2+}/EDTA and cleaved by Fe^{2+} at the same time are shown as red triangles. The paired regions [76] are represented by Pn or Pn′ (5′ or 3′ strands of a pairing, respectively) at the top of the figure and are color coded as in Figure 8.

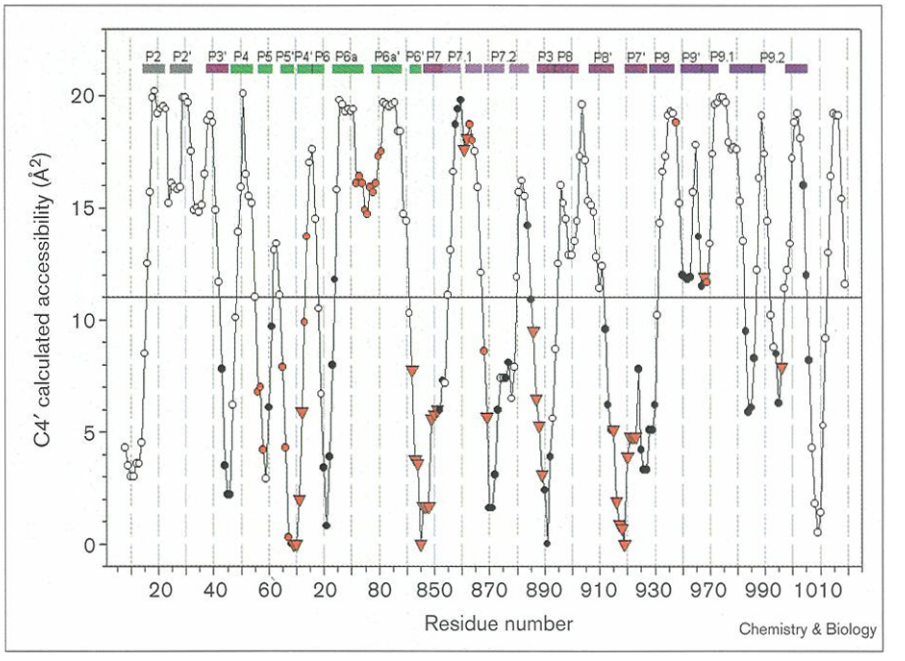

Figure 8

Fe^{2+} cleavage sites in the bacteriophage T4-derived *td* intron. **(a)** Stereo drawing of a global view of the *td* intron. Only the RNA backbone is represented and the various subdomains are color-coded and indicated. The two metals 'A' and 'B' at the catalytic site are colored in yellow and orange, respectively. The Fe^{2+}-cleavage sites are indicated by cyan spheres, with the sphere size representing the extent of cleavage by Fe^{2+}. The P1P2 region is displayed in grey, the P6P4P5 region in green, the P8P3P7 region is shown in crimson and the P7 and P9 extensions are in pink and purple, respectively. **(b)** Stereo drawing of a local view of the catalytic core of the *td* intron. The view is from P1. Paired regions are shown in blue/green (P4, P5, P6) or purple/pink (P7), joining regions (J5/4, J6/7, J8/7) are colored grey with their bases omitted for reasons of clarity. Metal ions and Fe^{2+} cleavage sites are shown as in (a). These drawings were produced using INSIGHT II (Biosym).

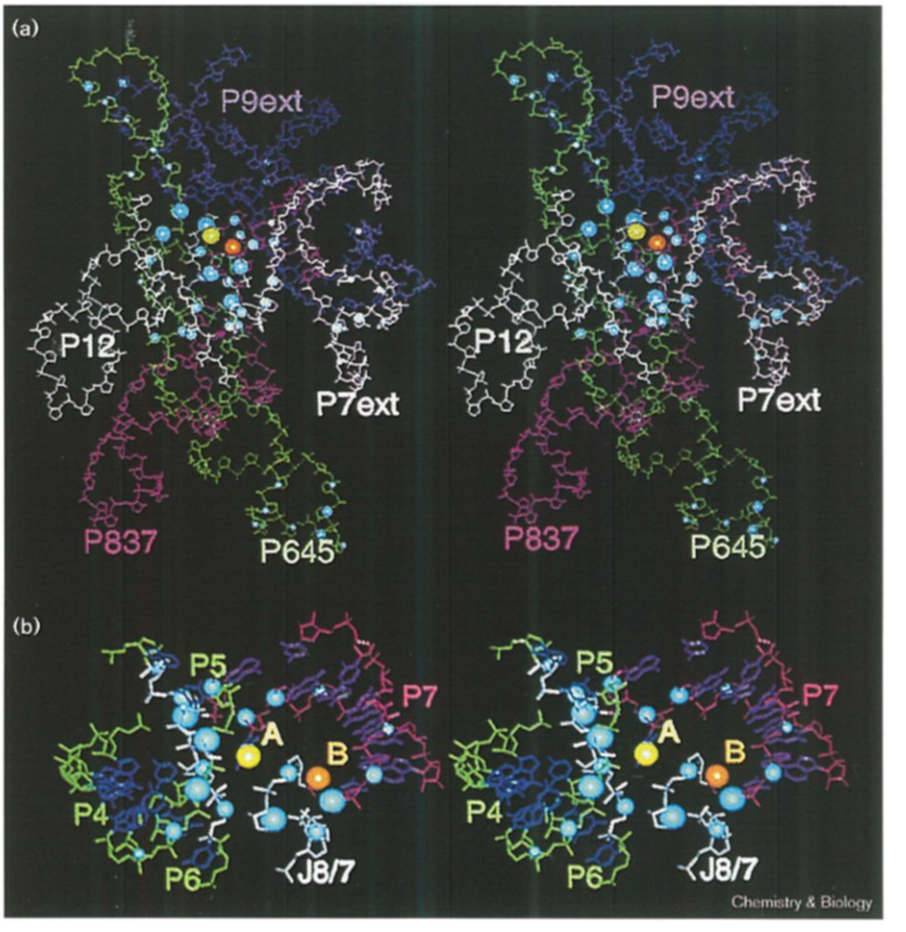

Figure 9

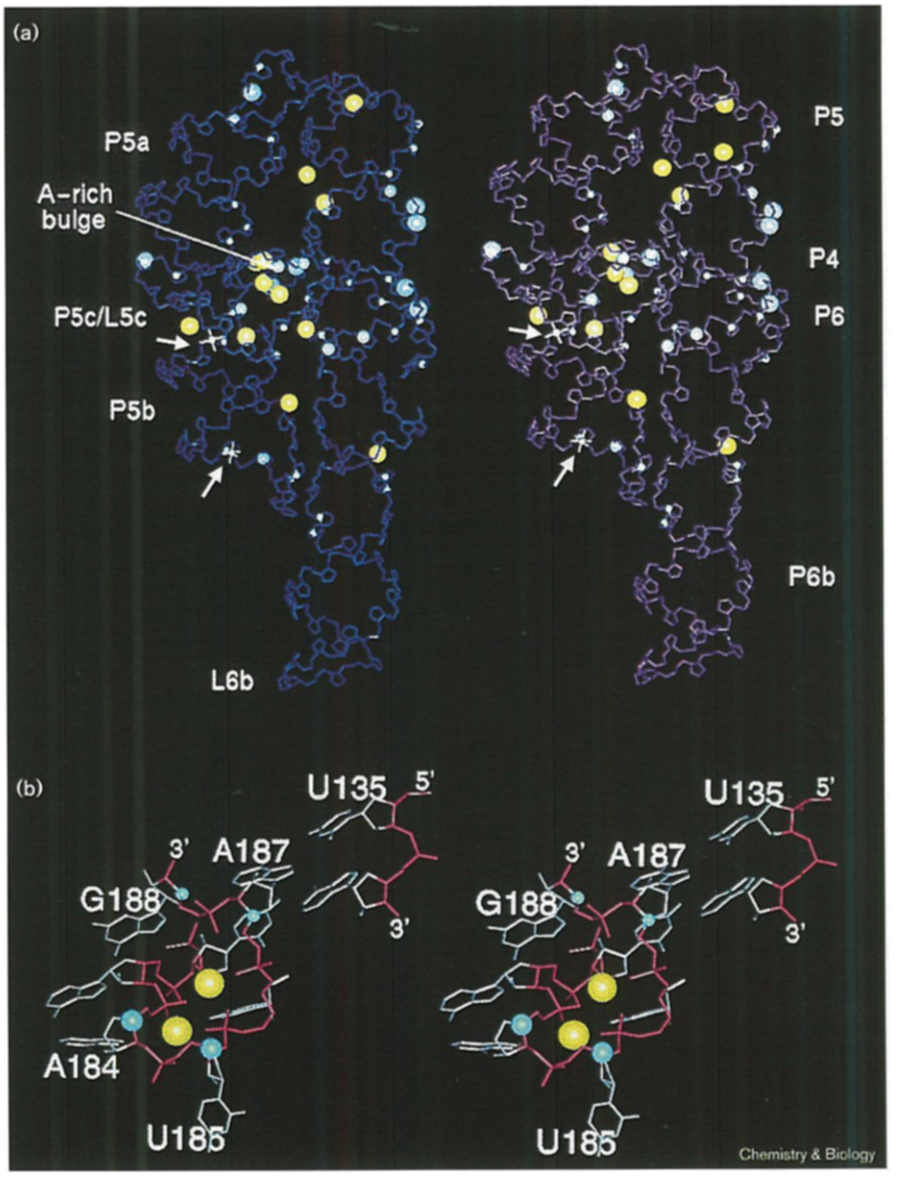

Fe^{2+} cleavage sites in the P4–P6 domain of the *Tetrahymena thermophila* LSU group I intron. **(a)** Backbone representation of the two P4–P6 domain molecules in the asymmetric unit of the crystal structure (PDB code: 1GID). Several secondary structure elements are indicated on the side. The divalent metals identified in Cate *et al.* [8] are shown as yellow spheres, two cobalt hexammine sites [48] as grey ball and stick representations, and the Fe^{2+}-cleavage sites as cyan spheres with the sphere size corresponding to the intensity of cleavage by Fe^{2+}. **(b)** Stereo drawing of the A-rich bulge with the Fe^{2+}-cleavage sites (cyan) and the two divalent metals (yellow) that coordinate the phosphate groups. The size of the spheres corresponds to the extent of cleavage by Fe^{2+}. The base pairs U135–A187 and A136–U182 are also shown. These drawings were produced using INSIGHT II (Biosym).

applicable to RNAs requiring divalent metal ions for folding or activity or both.

Significance

A major challenge in studying catalytic RNA is to locate the structurally and functionally important divalent metal ions required for folding and/or catalysis. We applied a method commonly used for mapping metal-ion-binding sites in proteins and protein–ligand complexes to the well-characterized group I intron family of catalytic RNAs. The method is based on the observations that Fe^{2+} can replace Mg^{2+} structurally and/or functionally and that Fe^{2+} can generate highly reactive and short-lived cleavage agents via the Fenton reaction. Cleavage by Fe^{2+} occurs in distinct regions of the group I intron RNA and is only observed with native RNA. It can be competed by Mg^{2+}, indicating that both ions interact with the same or overlapping binding sites. In a three-dimensional model of the bacteriophage T4-derived *td* intron, cleavage sites separated in the secondary structure come together in three-dimensional space to form metal-ion-binding pockets. There is very good agreement between nucleotides cleaved by Fe^{2+} and nucleotides close to metal ions determined using X-ray crystallography. This is also the case for positions in which phosphorothioate substitutions lead to reduced activity and for nucleotides cleaved by metal-hydroxyl groups. The method is therefore a tool to confirm published metal-ion-binding sites, as well as to detect new binding pockets for metal ions. It should, in principle, be applicable to all RNAs in which metal ions play an

important structural and/or functional role. By combining the experimental data obtained from Fe^{2+}-mediated cleavage, from phosphorothioate interference/'manganese rescue' experiments, and from metal-hydroxyl cleavage sites, with the existing three-dimensional models of catalytic RNAs, it should be possible to localize and model metal-ion-binding sites. This will increase our understanding of how metal ions assist RNAs in maintaining their native fold and performing catalysis.

Material and methods

Materials and general methods

All chemicals were obtained from Boehringer Mannheim, Fluka, Merck, Roth or Sigma and were of the highest purity available. Enzymes for restriction, modification, or synthesis of DNA and RNA were obtained from New England Biolabs and Pharmacia. Manipulation of DNA and 5′ end-labelling of RNA were as described previously [71]. RNA was labelled at its 3′-end using [α^{32}P]cordycepin and yeast poly(A) polymerase (Amersham) [72]. Sequencing ladders were generated by limited hydrolysis with RNase T1 and $NaHCO_3$ [73].

Plasmids and preparation of RNA

The plasmids containing the phage T4-derived *td*L-7 and *sunY*L–13 introns have been described previously [48]; the plasmid pBGST7 [74] was the source for the *Tetrahymena thermophila* LSU intron. A ribozyme template lacking the first 21 nucleotides was generated by amplification in a standard PCR using the primers Tth5′L-21: 5′-TAATACGACTCACTATAGGAGGGAAAAGTTATCAG-3′ and the M13 sequencing primer #1212 (New England Biolabs). The conditions of the T7 run-off transcription (40 mM Tris–HCl, pH 8.0; 13 mM $MgCl_2$; 40 mM NaCl; 2 mM spermidine; 10 mM NTPs; 12.5 mM dithiothreitol; 50 ng/μl template DNA; 2.5 U/μl T7 RNA polymerase; 4 h at 37°C) were adjusted, so that all three introns underwent self-catalyzed hydrolysis at their 3′-splice sites [75] producing the ribozymes used in the analyses. RNA was purified from 5%-polyacrylamide (39:1 acrylamide:bisacrylamide) gels containing 7 M urea, visualized by UV shadowing or autoradiography, and eluted into 10 mM Tris–HCl, pH 8.0; 250 mM NaCl; 2 mM EDTA; 0.1% SDS. After elution, the RNA was precipitated with ethanol, resuspended in bi-distilled water and stored at –20°C.

Hydroxyl radical cleavage reactions

The procedure described for Fe^{2+}/EDTA cutting of DNA [58] was used for RNA cleavage with minor modifications. Hydroxyl radical cleavage experiments were repeated three to seven times with different RNA preparations.

Fe^{2+}-mediated cleavage. For experiments with native RNA, 1 μl RNA (5 pmol; approximately 50,000 cpm) was added to 1 μl 5 × native cleavage buffer (1 × NCB: 25 mM Mops–KOH, pH 7.0; 3 mM $MgCl_2$; 400 μM spermidine; the 1 × cleavage buffer additionally included 200 mM NaCl for the *Tetrahymena* LSU intron and 50 mM NH_4Cl for the *sunY* intron), incubated for 2 min at 56°C, followed by 3 min incubation at room temperature. 1 μl of 1.25 mM $FeCl_2$ was added to the reaction tube, mixed by centrifugation and incubated for 1 min before adding 1 μl 12.5 mM sodium ascorbate. After 1 min, 1 μl of 12.5 mM H_2O_2 was added to initiate the reaction and rapidly mixed. The final concentrations were 250 μM for Fe^{2+} and 2.5 mM for both sodium ascorbate and hydrogen peroxide.

In the Mg^{2+}-competition experiments, $MgCl_2$ was added as a 5 × stock solution of the final Mg^{2+}-concentration given in Figure 2 to the 1.25 mM $FeCl_2$ solution. The Fe^{2+}/Mg^{2+} mixture was then pipetted into the reaction tube and the cleavage reaction continued as above.

For experiments with denatured RNA, 1 μl RNA (5 pmol; approximately 50,000 cpm) was added to 1 μl 5 × denaturing cleavage buffer (1 × DCB: 25 mM Mops–KOH, pH 7.0), incubated for 2 min at 90° C and immediately placed on ice. The cleavage reaction was performed as with native RNA, only the final concentrations used were 10 μM for Fe^{2+} and 100 μM for both sodium ascorbate and hydrogen peroxide.

The cleavage reaction was stopped after 45 s by the addition of 1 μl 1 M *thio*-urea, 1 μl glycogen (10 μg/μl) and 30 μl ethanol. The RNA was precipitated, resuspended in gel loading buffer (7 M urea; 0.01% bromophenol blue and xylenecyanol each) and electrophoresed in denaturing 6–8% polyacrylamide sequencing gels. The gels were dried and autoradiographed. Fe^{2+}-cleavage products were identified by visual inspection and then confirmed and quantified by phosphorimager analysis (Fuji, BAS2000; Molecular Dynamics). Strong, intermediate and weak cleavage sites were defined as having more than 50%, between 25–50%, and 10–25% of the signal strength of the cleavage band with the maximum intensity. The typical background cleavage intensity was about 5% of the maximum cleavage intensity.

Fe^{2+}/EDTA cleavage. 1 μl RNA (5 pmol; approximately 50,000 cpm) was added either to 1 μl 6 × NCB and renatured (see above), or to 1 μl 6 × DCB and denatured (see above). 1 μl each of 1.25 mM ammonium iron(II) sulfate and 2.5 mM EDTA were added to the reaction tube, mixed by centrifugation and incubated for 1 min. To initiate the reaction, 1 μl each of 12.5 mM sodium ascorbate and 25 mM hydrogen peroxide were added and rapidly mixed. The reaction was stopped after 3 min by the addition of 1 μl 1 M *thio*-urea, 10 μg glycogen and 30 μl ethanol. The RNA was precipitated and treated as above. Protected regions were first identified by visual inspection and then confirmed and quantified by phosphorimager analysis.

Acknowledgements

We thank Dolly Wittberger and Uwe von Ahsen for aesthetic inspiration and stimulating discussions, and Christina Waldsich for critically reading the manuscript. We also thank Eric Westhof for the coordinates of the T4 *td* intron and for calculating the solvent accessibilities of the C4′ atoms, Bryn Weiser for the XRNA program, and Jamie Cate and Jennifer Doudna for sending us the coordinates of the *Tetrahymena* P4–P6 domain prior to their release in the protein database. This work was supported by the Austrian Science Foundation (FWF) through grants P11362 and P11999 to R.S., the Deutsche Forschungsgemeinschaft and the Fonds der chemischen Industrie.

References

1. Pan, T., Long, D.M. & Uhlenbeck, O.C. (1993) Divalent metal ions in RNA folding and catalysis. In *The RNA World* (Gesteland, R.F. & Atkins, J.F., eds), pp. 271-302, Cold Spring Harbor Laboratory Press, Cold Spring Harbor.
2. Pyle, A.M. (1993). Ribozymes: A distinct class of metalloenzymes. *Science* **261**, 709-714.
3. Yarus, M. (1993). How many catalytic RNAs? Ions and the Cheshire cat conjecture. *FASEB J.* **7**, 31-39.
4. Streicher, B. & Wallis, M.G. (1996) Metal ions as the key to the functioning of both the group I intron and the ribosome. In *Ribosomal RNA and Group I Introns* (Green, R. & Schroeder, R., eds), pp. 103-128, R.G. Landes, Austin.
5. Jack, A., Ladner, J.E., Rhodes, D., Brown, R.S. & Klug, A. (1977). A crystallographic study of metal-binding to yeast $tRNA^{Phe}$. *J. Mol. Biol.* **111**, 315-318.
6. Pley, H.W., Flaherty, K.M. & McKay, D.B. (1994). Three-dimensional structure of a hammerhead ribozyme. *Nature* **372**, 68-74.
7. Scott, W.G., Murray, J.B., Arnold, J.R.P., Stoddard, B.L. & Klug, A. (1996). Capturing the structure of a catalytic RNA intermediate: the hammerhead ribozyme. *Science* **274**, 2065-2069.
8. Cate, J.H., *et al.*, & Doudna, J.A. (1996). Crystal structure of a group I ribozyme domain: principles of RNA packing. *Science* **273**, 1678-1685.
9. Correll, C.C., Freeborn, B., Moore, P.B. & Steitz, T.A. (1997). Metals, motifs, and recognition in the crystal structure of a 5S rRNA domain. *Cell* **91**, 705-712.
10. Dahm, S.C. & Uhlenbeck, O.C. (1991). Role of divalent metal ions in the hammerhead RNA cleavage reaction. *Biochemistry* **30**, 9464-9469.
11. Christian, E.L. & Yarus, M. (1993). Metal coordination sites that contribute to structure and catalysis in the group I intron from *Tetrahymena*. *Biochemistry* **32**, 4475-4480.

12. Harris, M.E. & Pace, N.R. (1995). Identification of phosphates involved in catalysis by the ribozyme RNase P RNA. *RNA* **1**, 210-218.
13. Cate, J.H., Hanna, R.L. & Doudna, J.A. (1997). A magnesium ion core at the heart of a ribozyme domain. *Nat. Struct. Biol.* **4**, 553-558.
14. Brown, R.S., Hingerty, B.E., Dewan, J.C. & Klug, A. (1983). Pb(II)-catalysed cleavage of the sugar-phosphate backbone of yeast $tRNA^{Phe}$ – implications for lead toxicity and self-splicing RNA. *Nature* **303**, 543-546.
15. Marciniec, T., Ciesiolka, J., Wresinski, J. & Krzyzosiak, W. (1989). Identification of the magnesium, europium and lead binding sites in *E. coli* and lupine $tRNA^{Phe}$ by specific metal ion-induced cleavages. *FEBS Lett.* **243**, 293-298.
16. Streicher, B., von Ahsen, U. & Schroeder, R. (1993). Lead cleavage sites in the core structure of group I intron-RNA. *Nucleic Acids Res.* **21**, 311-317.
17. Zito, K., Hüttenhofer, A. & Pace, N.R. (1993). Lead-catalyzed cleavage of ribonuclease P RNA as a probe for integrity of tertiary structure. *Nucleic Acids Res.* **21**, 5916-5920.
18. Streicher, B., Westhof, E. & Schroeder, R. (1996). The environment of two metals ions surrounding the splice site of a group I intron. *EMBO J.* **15**, 2556-2564.
19. Bassi, G.S., Møllegaard, N.E., Murchie, A.I., von Kitzing, E. & Lilley, D.M. (1995). Ionic interactions and the global conformations of the hammerhead ribozyme. *Nat. Struct. Biol.* **2**, 45-55.
20. Celander, D.W. & Cech, T.R. (1991). Visualizing the higher order folding of a catalytic RNA molecule. *Science* **251**, 401-407.
21. Brown, I.B. (1988). What factors determine cation coordination numbers? *Acta Crystallogr. Sect. B* **44**, 545-553.
22. Glusker, J.P. (1991). Structural aspects of metal liganding to functional groups in proteins. *Adv. Protein Chem.* **42**, 1-76.
23. Udenfried, S., Clark, C.T., Axelrod, J. & Brodie, R.B. (1954). Ascorbic acid in aromatic hydroxylation I. A model system for aromatic hydroxylation. *J. Biol. Chem.* **208**, 731-739.
24. Burkhoff, A.M. & Tullius, T.D. (1987). The unusual conformation adopted by the adenine tracts in kinetoplast DNA. *Cell* **48**, 935-943.
25. Tullius, T.D. & Dombroski, B.A. (1985). Iron(II) EDTA used to measure the helical twist along any DNA molecule. *Science* **230**, 679-681.
26. Tullius, T.D. & Dombroski, B.A. (1986). Hydroxyl radical 'footprinting': high-resolution information about DNA–protein contacts and application to lambda repressor and Cro protein. *Proc. Natl Acad. Sci. USA* **83**, 5469-5473.
27. Powers, T. & Noller, H.F. (1995). Hydroxyl radical footprinting of ribosomal proteins on 16S rRNA. *RNA* **1**, 194-209.
28. Hertzberg, R.P. & Dervan, P.B. (1984). Cleavage of DNA with Methidiumpropyl-EDTA-Iron(II): reaction conditions and product analyses. *Biochemistry* **23**, 3934-3945.
29. Mah, S.C., Townsend, C.A. & Tullius, T.D. (1994). Hydroxyl radical footprinting of calicheamicin. Relationship of DNA binding to cleavage. *Biochemistry* **33**, 614-621.
30. Latham, J.A. & Cech, T.R. (1989). Defining the inside and outside of a catalytic RNA molecule. *Science* **245**, 276-282.
31. Farber, J.M. & Levine, R.L. (1986). Sequence of a peptide susceptible to mixed-function oxidation. Probable cation binding site in glutamine synthetase. *J. Biol. Chem.* **261**, 4574-4578.
32. Wei, C.H., Chou, W.Y. & Chang, G.G. (1995). Identification of Asp258 as the metal coordinate of pigeon liver malic enzyme by site-specific mutagenesis. *Biochemistry* **34**, 7949-7954.
33. Mustaev, A., Kozlov, M., Markovtsov, V., Zaychikov, E., Denissova, L. & Goldfarb, A. (1997). Modular organization of the catalytic center of RNA polymerase. *Proc. Natl Acad. Sci. USA* **94**, 6641-6645.
34. Soundar, S. & Colman, R.F. (1993). Identification of metal-isocitrate binding site of pig heart NADP- specific isocitrate dehydrogenase by affinity cleavage of the enzyme by Fe^{2+}-isocitrate. *J. Biol. Chem.* **268**, 5264-5271.
35. Ettner, N., *et al.*, & Hillen, W. (1995). Proximity mapping of the Tet repressor-tetracycline-Fe^{2+} complex by hydrogen peroxide mediated protein cleavage. *Biochemistry* **34**, 22-31.
36. Zaychikov, E., *et al.*, & Mustaev, A. (1996). Mapping of catalytic residues in the RNA polymerase active center. *Science* **273**, 107-109.
37. Lykke-Andersen, J., Garrett, R.A. & Kjems, J. (1997). Mapping metal ions at the catalytic centres of two intron-encoded endonucleases. *EMBO J.* **16**, 3272-3281.
38. Grosshans, C.A. & Cech, T.R. (1989). Metal ion requirements for sequence-specific endoribonuclease activity of the *Tetrahymena* ribozyme. *Biochemistry* **28**, 6888-6894.
39. Wang, J.-F. & Cech, T.R. (1992). Tertiary structure around the guanosine-binding site of the *Tetrahymena* ribozyme. *Science* **256**, 526-529.
40. Zhong, M. & Kallenbach, N.R. (1994). Mapping tRNA and 5S RNA tertiary structures by charge dependent Fe(II)-catalyzed cleavage. *J. Biomol. Struct. Dyn.* **11**, 901-911.
41. Christian, E.L. & Yarus, M. (1992). Analysis of the role of phosphate oxygens in the group I intron from *Tetrahymena*. *J. Mol. Biol.* **228**, 743-758.
42. Piccirilli, J.A., Vyle, J.S., Caruthers, M.H. & Cech, T.R. (1993). Metal ion catalysis in the *Tetrahymena* ribozyme reaction. *Nature* **361**, 85-88.
43. Sjögren, A.S., Pettersson, E., Sjöberg, B.M. & Strömberg, R. (1997). Metal ion interaction with cosubstrate in self-splicing of group I introns. *Nucleic Acids Res.* **25**, 648-653.
44. McConnell, T.S., Herschlag, D. & Cech, T.R. (1997). Effects of divalent metal ions on individual steps of the *Tetrahymena* ribozyme reaction. *Biochemistry* **36**, 8293-8303.
45. Weinstein, L.B., Jones, B.C.N.M., Cosstick, R. & Cech, T.R. (1997). A second catalytic metal ion in a group I ribozyme. *Nature* **388**, 805-808.
46. Jaeger, L., Westhof, E. & Michel, F. (1993). Monitoring of the cooperative unfolding of the *sunY* group I intron of bacteriophage T4. The active form of the *sunY* ribozyme is stabilized by multiple interactions with 3′ terminal intron components. *J. Mol. Biol.* **234**, 331-346.
47. Lehnert, V., Jaeger, L., Michel, F. & Westhof, E. (1996). New loop-loop tertiary interactions in self-splicing introns of subgroup IC and ID: a complete 3D model of the *Tetrahymena thermophila* ribozyme. *Chem. Biol.* **3**, 993-1009.
48. Cate, J.H. & Doudna, J.A. (1996). Metal-binding sites in the major groove of a large ribozyme domain. *Structure* **4**, 1221-1229.
49. Heuer, T.S., Chandry, P.S., Belfort, M., Celander, D.W. & Cech, T.R. (1991). Folding of group I introns from bacteriophage T4 involves internalization of the catalytic core. *Proc. Natl Acad. Sci. USA* **88**, 11105-11109.
50. Galloway Salvo, J.L., Coetzee, T. & Belfort, M. (1990). Deletion-tolerance and *trans*-splicing of the bacteriophage T4 *td* intron: Analysis of the P6–L6a region. *J. Mol. Biol.* **211**, 537-549.
51. Wank, H. & Schroeder, R. (1996). Antibiotic-induced oligomerisation of group I intron RNA. *J. Mol. Biol.* **258**, 53-61.
52. Inoue, T. & Cech, T.R. (1985). Secondary structure of the circular form of the *Tetrahymena* rRNA intervening sequence: a technique for RNA structure analysis using chemical probes and reverse transcriptase. *Proc. Natl Acad. Sci. USA* **82**, 648-652.
53. Michel, F., *et al.*, & Shub, D.A. (1992). Activation of the catalytic core of a group I intron by a remote 3′ splice junction. *Genes Dev.* **6**, 1373-1385.
54. Brenowitz, M.D., Senear, D.F., Shea, M.A. & Ackers, G.K. (1986). Quantitative DNase I footprint titration: a method for studying protein-DNA interactions. *Methods Enzymol.* **130**, 132-181.
55. Brown, R.S., Dewan, J.C. & Klug, A. (1985). Crystallographic and biochemical investigation of the lead(II)-catalyzed hydrolysis of yeast phenylalanine tRNA. *Biochemistry* **24**, 4785-4801.
56. Behlen, L.S., Sampson, J.R., DiRenzo, A.B. & Uhlenbeck, O.C. (1990). Lead-catalyzed cleavage of yeast $tRNA^{Phe}$ mutants. *Biochemistry* **29**, 2515-2523.
57. Rogers, J., Chang, A.H., von Ahsen, U., Schroeder, R. & Davies, J. (1996). Inhibition of the self-cleavage reaction of the human hepatitis delta virus ribozyme by antibiotics. *J. Mol. Biol.* **259**, 916-925.
58. Tullius, T.D., Dombroski, B.A., Churchill, M.E. & Kam, L. (1987). Hydroxyl radical footprinting: a high-resolution method for mapping protein-DNA contacts. *Methods Enzymol.* **155**, 537-558.
59. Celander, D.W. & Cech, T.R. (1990). Iron(II)-Ethylenediaminetetraacetic acid catalyzed cleavage of RNA and DNA oligonucleotides: similar reactivity toward single- and double-stranded forms. *Biochemistry* **29**, 1355-1361.
60. Brunel, C., Romby, P., Westhof, E., Ehresmann, C. & Ehresmann, B. (1991). Three-dimensional model of *Escherichia coli* ribosomal 5 S RNA as deduced from structure probing in solution and computer modeling. *J. Mol. Biol.* **221**, 293-308.
61. Michel, F. & Westhof, E. (1990). Modelling of the three-dimensional architecture of group I catalytic introns based on comparative sequence analysis. *J. Mol. Biol.* **216**, 585-610.
62. Laggerbauer, B., Murphy, F.L. & Cech, T.R. (1994). Two major tertiary folding transitions of the *Tetrahymena* catalytic RNA. *EMBO J.* **13**, 2669-2676.
63. Jaeger, L., Michel, F. & Westhof, E. (1994). Involvement of a GNRA tetraloop in long-range RNA tertiary interactions. *J. Mol. Biol.* **236**, 1271-1276.
64. Jaeger, J.A., Zuker, M. & Turner, D.H. (1990). Melting and chemical modification of a cyclized self-splicing group I intron: similarity of structures in 1 M Na^+, in 10 mM Mg^{2+}, and in the presence of substrate. *Biochemistry* **29**, 10147-10158.

65. Pyle, A.M., Murphy, F.L. & Cech, T.R. (1992). RNA substrate binding site in the catalytic core of the *Tetrahymena* ribozyme. *Nature* **358**, 123-128.
66. Williamson, C.L., Tierney, W.M., Kerker, B.J. & Burke, J.M. (1987). Site-directed mutagenesis of core sequence elements 9R', 9L, 9R, and 2 in self-splicing *Tetrahymena* pre-rRNA. *J. Biol. Chem.* **262**, 14672-14682.
67. Kieft, J.S. & Tinoco, I. (1997). Solution structure of a metal-binding site in the major groove of RNA complexed with cobalt (III) hexammine. *Structure* **5**, 713-721.
68. Prigodich, R.V. & Martin, C.T. (1990). Reaction of single-stranded DNA with hydroxyl radical generated by Iron(II)-Ethylenediaminetetraacetic acid. *Biochemistry* **29**, 8017-8019.
69. Henle, E.S., Luo, Y., Gassmann, W. & Linn, S. (1996). Oxidative damage to DNA constituents by iron-mediated Fenton reactions. The deoxyguanosine family. *J. Biol. Chem.* **271**, 21177-21186.
70. Luo, Y., Henle, E.S. & Linn, S. (1996). Oxidative damage to DNA constituents by iron-mediated Fenton reactions. The deoxycytidine family. *J. Biol. Chem.* **271**, 21167-21176.
71. Sambrook, J., Fritsch, E.F. & Maniatis, T. (1989). *Molecular Cloning: A Laboratory Manual* (2nd edn.). Cold Spring Harbor Laboratory Press, Cold Spring Harbor.
72. Lingner, J. & Keller, W. (1993). 3'-end labeling of RNA with recombinant yeast poly(A) polymerase. *Nucleic Acids Res.* **21**, 2917-2920.
73. Donis-Keller, H., Maxam, A.M. & Gilbert, W. (1977). Mapping adenines, guanines and pyrimidines in RNA. *Nucleic Acids Res.* **4**, 2527-2538.
74. Been, M.D. & Cech, T.R. (1986). One binding site determines sequence specificity of *Tetrahymena* pre-rRNA self-splicing, trans-splicing, and RNA enzyme activity. *Cell* **47**, 207-216.
75. Inoue, T., Sullivan, F.X. & Cech, T.R. (1986). New reactions of the ribosomal RNA precursor of *Tetrahymena* and the mechanism of self-splicing. *J. Mol. Biol.* **189**, 143-165.
76. Burke, J.M., *et al.*, & Tabak, H.W. (1987). Structural conventions for group I introns. *Nucleic Acids Res.* **15**, 7217-7221.
77. Cech, T.R., Damberger, S.H. & Gutell, R.R. (1994). Representation of the secondary and tertiary structure of group I introns. *Nat. Struct. Biol.* **1**, 273-280.
78. Richmond, T.J. (1984). Solvent accessible surface area and excluded volume in proteins. Analytical equations for overlapping spheres and implications for the hydrophobic effect. *J. Mol. Biol.* **178**, 63-89.

Because *Chemistry & Biology* operates a 'Continuous Publication System' for Research Papers, this paper has been published via the internet before being printed. The paper can be accessed from http://biomednet.com/cbiology/cmb – for further information, see the explanation on the contents pages.